LABORATORY MODEL TEST ON GEOSYNTHETIC-REINFORCED EMBANKMENTS ON PEAT LAND AND DEGRADED PERMAFROST

N. Mohidin[1] and M. Alfaro[2]
[1]Department of Civil Engineering, University of Manitoba, Canada; Tel: 1-204-474-8072; Fax: 1-204-474-7513; Email: ummohidi@cc.umanitoba.ca
[2]Department of Civil Engineering, University of Manitoba, Canada; Tel: 1-204-474-8155; Fax: 1-204-7513; Email: Marolo.Alfaro@ad.umanitoba.ca

ABSTRACT

Climate warming and human activities can lead to increases in the temperature of permafrost and to thawing. In regions of discontinuous permafrost, thawing may produce thickening of the active layer, large settlements and non-recoverable shear deformations in soft foundations such as peats and clays frequently found in Northern Canada. The use of geosynthetics reinforcements has been considered as one of the adaptation strategies for roads and railways impacted by climate change. It is important to improve the understanding of the operating mechanisms of both reinforced and unreinforced embankments on thawed peat land and degraded permafrost. This paper presents the results of a laboratory experimental study on the deformations patterns of foundation beneath geosynthetic-reinforced and unreinforced embankments. Artificial transparent clay that has similar properties with that of soft soils represents the foundation material. The monitoring system consists of a laser source that optically slices the transparent clay and a high-resolution digital camera that captures the images of soil deformations. Spatial deformations beneath the embankment were determined using Particle Image Velocimetry (PIV) technique. Results of this study provide insight into the nature of deformations and mechanisms producing functional failure of embankments on peat land and degraded permafrost.

Keywords: Geosynthetics, highway embankment, climate warming, laboratory model test, deformations.

INTRODUCTION

Northern Canada is rich in mineral, petro-carbon, and hydroelectric resources that will require future infrastructure projects. It is home to many First Nations communities. Additional roads and railways will have to be constructed into northern Canadian communities over soils with engineering properties that may degrade with climate change and land-use. Design and maintenance of this new infrastructure will have to take account of future warming over the anticipated life of these projects.

Construction of highway fills in Northern Canada currently follows similar practices to those used in warmer regions. Fill materials typically have higher thermal conductivity than the native soil. In addition, construction of roadways and other infrastructure removes vegetation cover, affects snow cover, increases heat transfer, and alters drainage patterns. This contributes significantly to disturbance of discontinuous permafrost, encountered within the northern part of some Canadian provinces and the southern part of northern territories (Fig. 1). Discontinuous permafrost regions correspond approximately to an isotherm with a current mean annual air temperature (MAAT) of 0ºC. Figure 2 shows the comparison between the isotherm of recent mean annual air

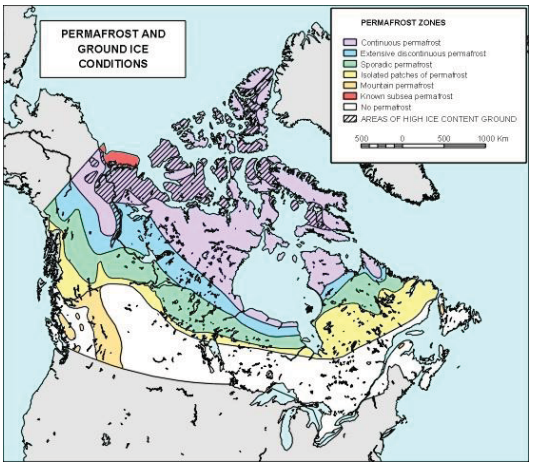

Fig. 1 Permafrost distribution in Canada.

temperature and that of 50 years ago. It can be shown that the zero degree isotherm has retreated towards the north. The warming of air temperature indicates warming of ground temperatures.

The soil deposits in northern Canada are predominantly peats and clays. For example, the northern part of central Canada has wide distribution of peat land as shown in Fig. 3. Construction of transportation infrastructure over these types of deposits is often very challenging. Climate change

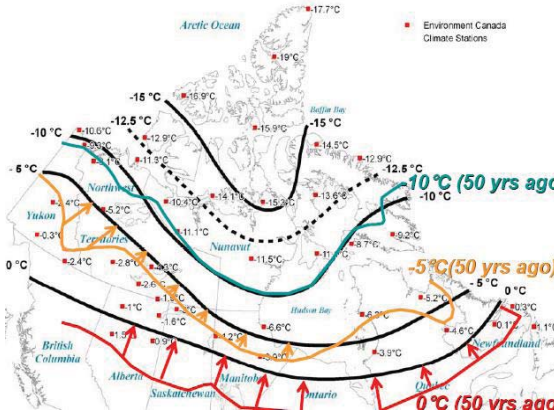

Fig. 2 Mean annual air temperature

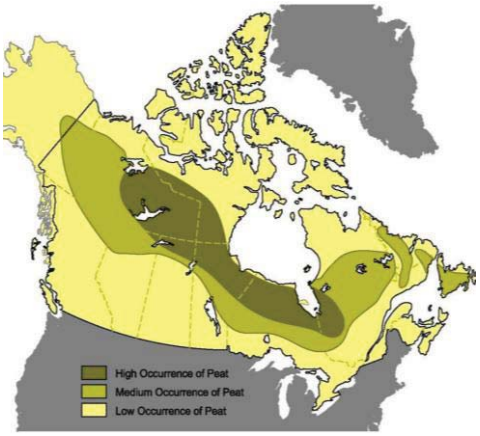

Fig. 3 Peat land distribution in Canada.

provides an added cause for concern. Expected changes in meteorological conditions, precipitation, solar radiation, wind speed, and other factors will induce temperature changes at ground level and at greater depths. These changes will affect civil engineering infrastructure, particularly in areas of discontinuous permafrost and frozen peat land. In these regions, thawing may produce increased pore water pressures, reduced strengths, differential settlements and non-recoverable shear deformations in soft foundations. Figures 4 and 5 show functional failures of road and railway associated with degrading permafrost and thawed peat land.

Manitoba Infrastructure and Transportation (MIT) faces increasing maintenance costs, reconstruction of damaged structures, and the replacement of many of its northern roads. To improve design and maintenance procedures, MIT and the University of Manitoba (UM) are collaborating on several projects that involve field instrumentation, laboratory testing and numerical modeling. The use of geosynthetic reinforcement has been considered as one of the adaptation strategies for roads and railways impacted by climate change.

Fig. 4 Excessive settlement and lateral movement of a road on degraded permafrost along Provincial Road 391 in Manitoba.

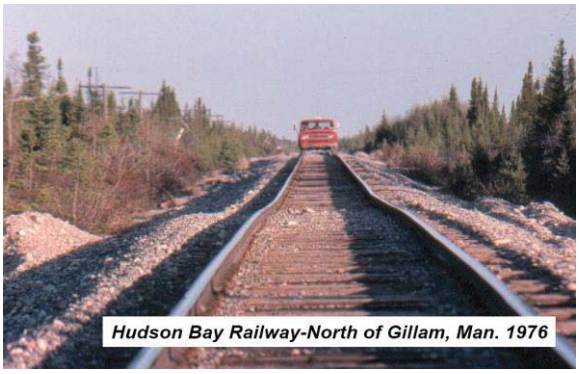

Fig. 5 Uneven settlement of a railway line on thawed peat land in Manitoba.

This paper presents the results of a laboratory experimental study on the deformation patterns of foundation beneath geosynthetic-reinforced and unreinforced embankments.

GEOSYNTHETIC-REINFORCED EMBANKMENT

Geosynthetics can be very attractive for works involving embankments on soft foundation soils. There are some alternatives with regards to the installation of geosynthetic reinforcement layer inside the embankment (Palmiera 2012). Figure 6 presents two alternatives of installing geosynthetic reinforcements at the base of the embankment.

In this study, geocell base reinforcement (Figure 6a) and wrap-around base reinforcement (Fig. 6b) are investigated. These types of installation create a stiffer mass at the base of the embankment. They tend to reduce differential settlements that are common in embankments on peat land and degraded permafrost. They also tend to reduce lateral spreading of the infill soil and create a relatively stiffened mat that redistributes the embankment load

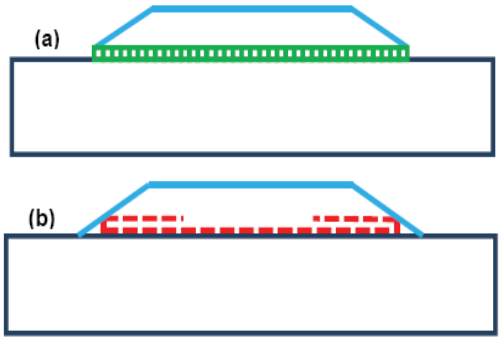

Fig. 6 Geosynthetic installation at the base of embankment: a) geocell, b) wrap-around.

over wider area on the underlying foundation, thereby giving rise to enhanced load carrying capacity and reduced deformations (Wesseloo et al. 2009).

LABORATORY MODEL TEST

Field tests and laboratory model tests are two approaches that are commonly used by many researches to investigate the deformations and failure mechanisms of embankments. Full-scale tests offer better understanding on the behaviour of the embankment and its foundation but can be expensive. Small-scale laboratory model tests provide a cost effective alternative.

Traditional model tests using natural clays are intrusive. Embedded sensors can influence the response of the embankment-foundation system, particularly for small-scale tests. Iskander and Liu, (2010) recommended the use of artificial transparent soil instead of real soils. The artificial soil can have similar properties of real soils. The use of see-through artificial soils gives good representation of the behaviour of foundations subjected to embankment loading.

Artificial transparent soils have been used successfully in laboratory model tests. Gill and Lehane (2001) studied pile penetration in clays using target tracing method. McKelvey, (2002) used transparent clay to investigate the failure mechanisms of stone columns in clay foundations. Liu (2003) used transparent clay to determine soil deformations under model footings in combination with digital image correlation technique.

Soil Materials

Transparent clay

The transparent synthetic clay used in this study has similar deformation properties to most natural clays and peats (see Mohidin et al. 2010). Amorphous silica and pore fluid were used to produce transparent clay. It consisted of ultrafine particle with individual diameter of 0.02 μm and surface area of 170 - 230 m^2/g. The refractive index, bulk density and tampered density for the silica powder determined in this study were 1.46, 20-130 kg/m^3 and 40 g/l, respectively. The specific gravity for this material had been reported to be around 2.1 (McKelvey 2002; Gill and Lehane 2001). Mannheimer and Oswald, (1993) estimated the amount of absorbed oil to be 2.1 cm^3 of pore fluid per gram of amorphous silica. The pore fluid was produced by mixing colourless mineral oil in normal paraffinic oil solvent. Both fluids were blended at 50:50 ratio by weight. The blend oil has a refractive index 1.464 at room temperature (about 20°C). The viscosity and density of the oil blend were 54.8 cP and 868 kg/m^3, respectively. Combination of this ratio produces the clearest end product of transparent synthetic soil.

Embankment soil

The soil used for the model embankment is poorly graded fine quartz sand with the following particle size properties: average particle size d_{50} = 0.65 mm; coefficient of curvature of gradation curve, C_c = 0.9; and coefficient of uniformity, C_u = 1.8. The maximum and minimum unit weights were 18 kN/m^3 and 16 kN/m^3, respectively. The shear strength of the sand was determined by performing conventional direct shear tests. Peak and critical internal friction angles were found to be 40° and 34°, respectively.

Geosynthetic Reinforcement

The wrap-around geosynthetic reinforcement used in this study is a non-woven Mirafi HP270 geotextile. The geocell reinforcement used the same material and was formed in diamond pattern similar to that used by other researchers (e.g., Krishnaswamy et al. 2000; Dash et al. 2001). Figure 7a shows the configuration of a geocell reinforcement specimen and Figure 7b shows that of a planar wrap-around reinforcement specimen. The diamond pattern of geocell produces lesser number of joints, and thus minimizing joint failure. The geocell has pocket dimensions of 12.5 mm x 25 mm (depth x height) and has aspect ratio (height to equivalent diameter ratio) of 0.5. This aspect ratio was recommended by other researches (Krishnaswamy et al. 2000, Mhaiskar and Mandal 1996) to provide maximum efficiency in terms of materials used. The joints in the geocell were made from commercially available 20 gauges hardware wire.

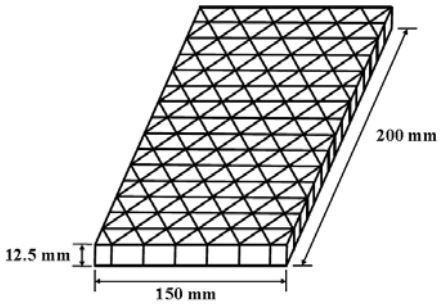

a) Geocell specimen

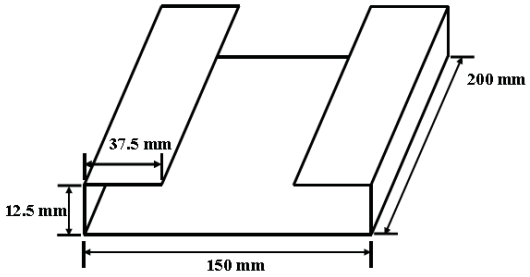

b) Wrap-around specimen

Fig. 7 Configurations of reinforcement specimen.

EXPERIMENTAL SETUP AND PROCEDURE

Optical Measurement in Transparent Clay

Particle Image Velocimetry (PIV) is a method of determining velocity fields from seeded flows. It has been used to measure soil deformation (e.g., Take et al. 2003). This method uses digital image correlation (DIC), which is a pattern recognition technique where two consecutive images are compared to obtain relative displacement and magnitude. The correlation function is used in DIC to locate the best matching position of two images to calculate body movements, deformations and velocity profiles.

In most practical geotechnical applications, DIC can provide sufficient resolution for analysis purposes (Iskander et al. 2002). PIV method has been successfully used for determining 2-D deformations under a footing in transparent soils (Liu 2003, Sadek et al. 2003). This technique has been adapted in this study to obtain the displacement fields under a model embankment.

The discrete form of standard correlation function, C is given by Iskander and Liu, (2010):

$$C(\Delta_x, \Delta_y) = \frac{1}{QR}\sum_{q=0}^{Q-1}\sum_{r=0}^{R-1} d(q,r)\, e(q+\Delta x, r+\Delta y) \quad (1)$$

where Q and R are dimensions in the two interrogated images, d and e are the grey scale intensities of two consecutive images being compared.

The correlation function will give a peak value located at the best matching ordinate throughout the function. The correlation function repetitively use shifting distances, Δ_x and Δ_y. If two functions, d(q,r) and e(q,r), have peak value of $C(x_1,y_1)$ at location (x_p,y_p), then the best match of both d(q,r) and e(q,r) occurs when e(q,r) is shifted from its origin located at (x_p,y_p).

For the larger image sizes, dividing them into sub-images or small interrogation windows is recommended. Cross-correlation is calculated to obtain peak values for each couple of corresponding interrogation windows. The complete displacement fields are determined from peak values at various interrogation windows.

Optical Test Setup

A Plexiglas tank with dimensions of 0.60 m x 0.20 m x 0.45 m (width x length x height) was used. Loading was applied using stepless compression testing machine beneath the tank. The load was applied through a rod and a rigid plate mounted at steel frame with a rate of 1 mm/min. LVDT and load cell were used to record the vertical displacement and load, respectively. The test setup is similar to the one used by Poungchompu et al., (2010), except that natural clay was used in their tests.

The setup, as shown in Fig. 8, consists of charge-couple device (CCD) camera, laser light source, line generator lens, loading system and a computer for automatic data acquisition and image processing. A line generator lens was used to produce an intense laser light sheet, which provided an improved illumination through the center section of the soil. A 40mW diode laser with a wavelength of 632.8 nm was used. A CCD camera with resolution of 1080 x 786 pixels was used to generate images.

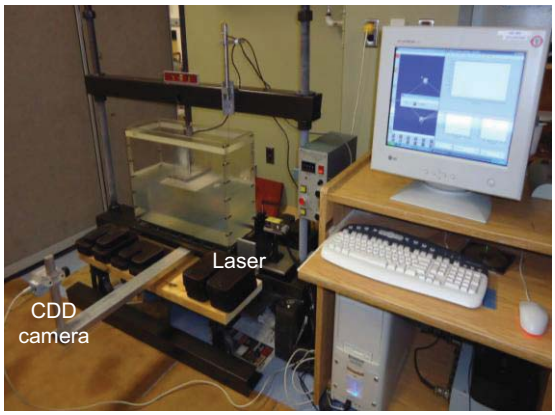

Fig. 8 Test setup of laboratory model test.

Distinctive speckle pattern (Fig. 9) is produced by the interaction between coherent laser light and transparent soils. The speckle pattern properties usually depend both on roughness and reflectance of

the surface (Iskander et al. 2002). This speckle pattern is created by coherent light beam, such as laser, scattered from a particle in a liquid that has well-defined spatial structure (Goodman 1975). Laser speckle technique was successfully applied to measure deformation patterns inside transparent soil models (Iskander and Liu 2010).

TEST RESULTS

Displacement Fields

Typical displacement fields, in this case of unreinforced embankment at failure, are shown in Fig. 10. Two consecutive images captured during loading were used to calculate the displacement fields. The arrows indicate the displacements of each interrogation window within the image. Only half of the image was shown due to symmetry. The displacements follow broadly the general bearing capacity failure mechanism. The displacement fields for reinforced embankments follow similar patterns with that of unreinforced embankment.

Pressure-Settlement Behaviour

Vertical pressure versus vertical displacement curves for unreinforced and reinforced embankments are shown in Fig. 11. Measured displacements and those obtained from PIV are shown in the figure. In the PIV method, the displacement is taken from the clay surface beneath the centreline of the embankment. The measured displacement is from the LVDT. The load was measured using load cell that was connected to the loading plate located at the top surface of the embankment. In Fig. 11, the solid lines are measured values while the dotted lines are those obtained from PIV method. The pressure-displacement relationships from PIV method are comparable with the measured ones, providing improved confidence about the PIV method.

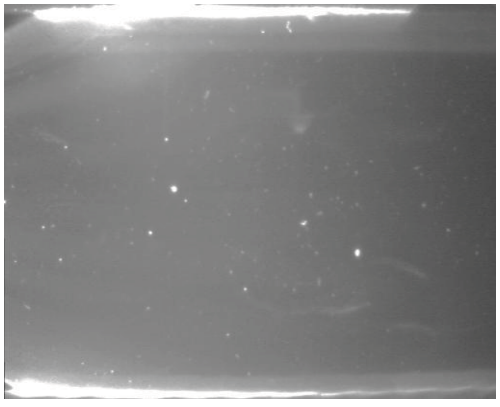

Fig. 9 Sample of distinctive speckle pattern.

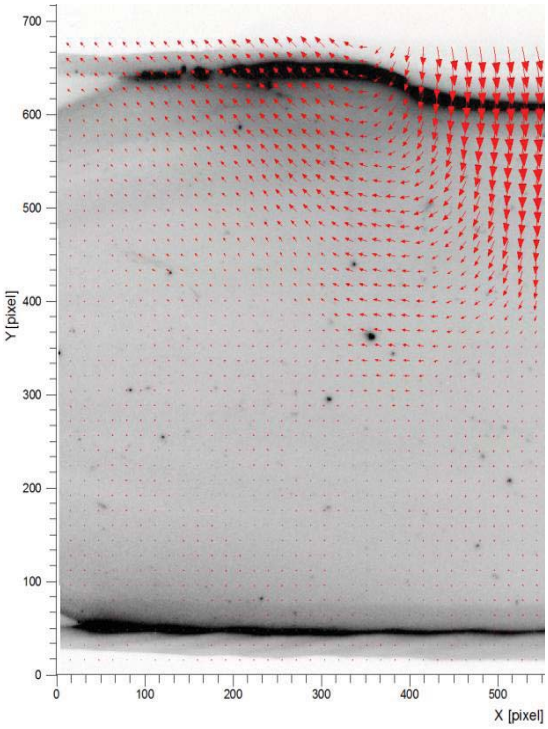

Fig. 10 Displacement fields at failure of unreinforced embankment.

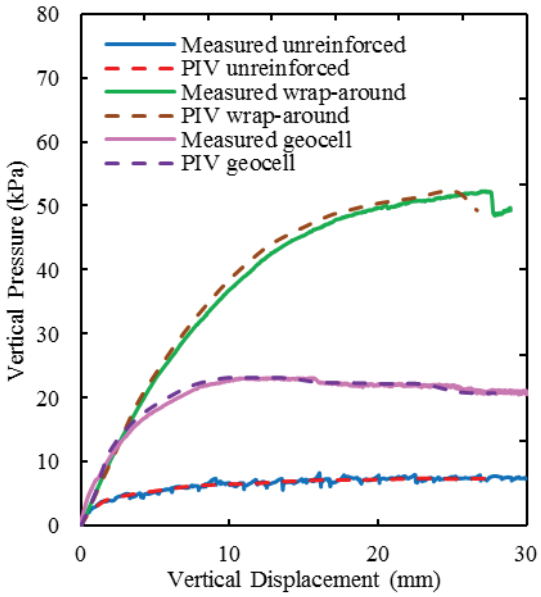

Fig. 11 Vertical pressure versus vertical displacement relationships.

The reinforced embankments show higher load carrying capacity than the unreinforced one. Wrap-around reinforcement provided higher capacity than

geocell reinforcement. These results are consistent with the results reported by Adam and Collins (1997) based on large-scale model tests. They found that load capacity of planar reinforced system is higher compared with geocell reinforced system.

In order to evaluate the load carrying capacity of reinforced embankments, a non-dimensional parameter called improvement factor (IF) has been proposed by Sitharam et al. (2007):

$$IF = \frac{q_r}{q_u} \quad (2)$$

where q_u = bearing pressure of unreinforced embankment and q_r = bearing pressure of geocell reinforced embankment. Both q_u and q_r are measured at the same vertical displacements. The improvement bearing pressure factors for geocell and wrap-around geosynthetic reinforcements plotted with vertical displacement are shown in Fig. 12. The provision of wrap-around reinforcement increased the improvement factor up to two times compared with geocell reinforcement, except at lower vertical displacements where the improvement factor for wrap-around reinforcement is lower than that of geocell reinforcement. The higher improvement factor of wrap-around reinforcement may be attributed to its better anchorage system above the embankment-foundation interface and higher tensile stiffness in compared to geocell reinforcement.

Vertical Displacements

Profiles for vertical displacements at selected stress levels of unreinforced, geocell-reinforced and wrap-around geosynthetic-reinforced embankments are shown in Figs. 13, 14 and 15, respectively. In

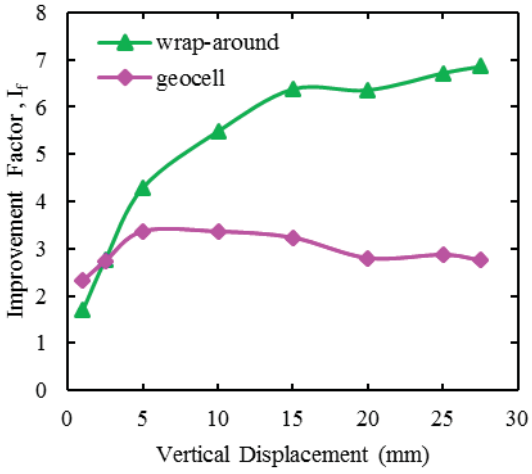

Fig. 12 Improvement factor versus vertical displacement.

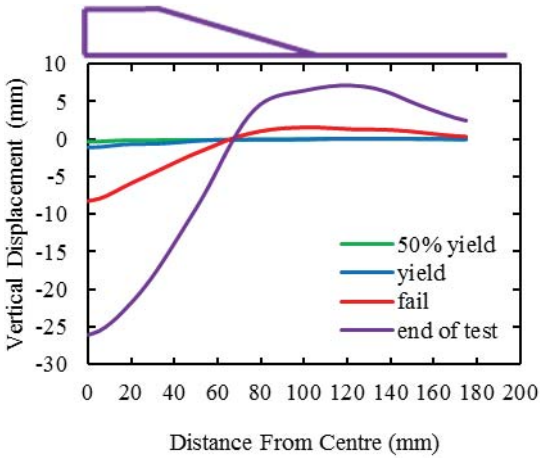

Fig. 13 Vertical displacement profile for unreinforced embankment.

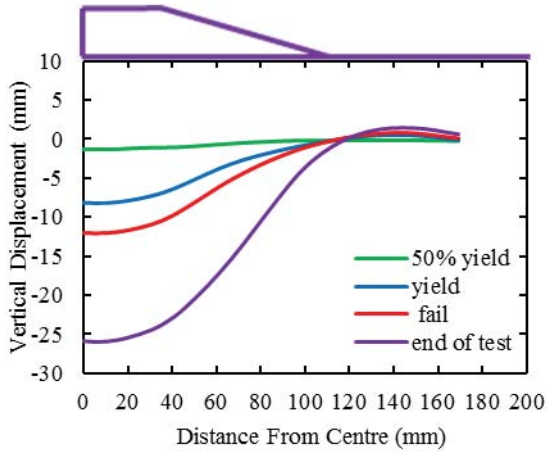

Fig. 14 Vertical displacement profile for reinforced embankment using geocell reinforcement.

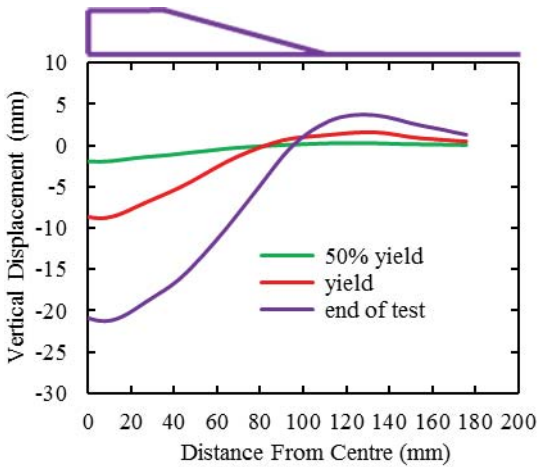

Fig. 15 Vertical displacement profile for reinforced embankment using wrap-around reinforcement.

these figures, deformations at 30 mm depth from the top clay surface were used. The yield condition in the figure refers to transition of pressure-displacement curves from elastic to plastic behaviour and the 50% of yield corresponds to half value of that yield pressure. The failure condition refers to condition when the slope for pressure-displacement curves tends to be horizontal or starting to decrease. The end of test refers to the condition when the test is terminated.

The shapes and patterns of the vertical displacement profile for unreinforced embankments has similar patterns with those reported by other investigators (e.g, Almeida et al. 1986, Indraratna et al. 1992). Figures 13, 14 and 15 show that heaving of the foundation beyond the toe of unreinforced embankment is relatively much higher compared to reinforced embankments. This is due mainly to the containment and confinement of the embankment by the reinforcement creating a better composite material that enhances the load carrying capacity of the system (Sitharam et al. 2005). The differential settlements in the embankment, particularly within the centreline and the crest, are higher in the case of unreinforced embankment. Geocell reinforcement seems to produce higher reduction than the wrap-around reinforcement. This is attributed to better ability of geocell in providing stiffened platform at the base of the embankment.

Horizontal Displacements

Typical horizontal displacements at the toe and mid-slope are shown in Figs. 16 and 17, respectively. They are expressed in terms of normalized depth (z/H) and normalized displacement (δ_h/H) where H is the height of the foundation layer, z is the depth, and δ_h is horizontal displacement. The horizontal displacements were compared at the corresponding vertical displacements of 25 mm. This displacement is at failure condition for reinforced and unreinforced embankments. The horizontal displacements beneath the mid-slope were found to be higher than beneath the toe. This is consistent with the results reported by Almeida et al. (1986). The inclusion of geocell and wrap-around geosynthetic reinforcements significantly reduces the outward lateral spreading of the soft clay foundation. The difference in reduction between the two types of reinforcements is very close.

CONCLUSIONS

The use of transparent clay in laboratory model tests improves the understanding about the operating mechanisms of both reinforced and unreinforced

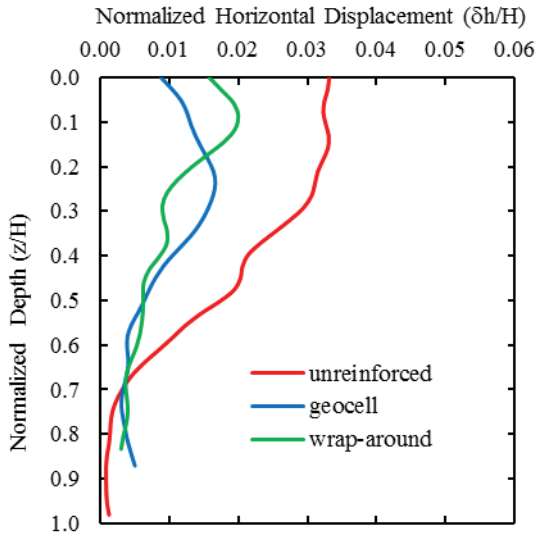

Fig. 16 Horizontal at the toe for unreinforced and reinforced embankment.

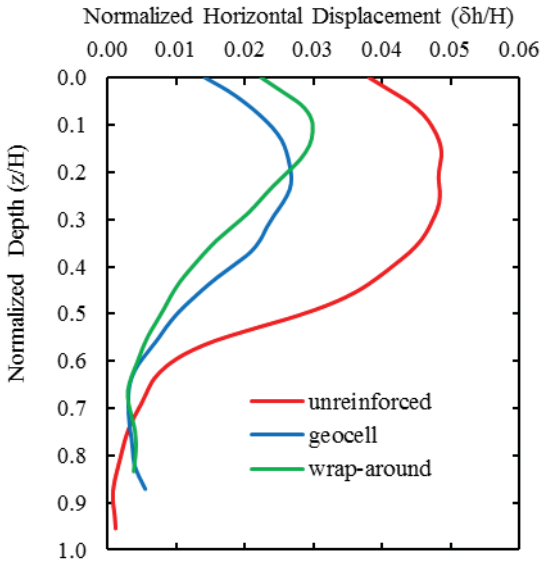

Fig. 17 Horizontal at the mid-slope for unreinforced and reinforced embankment.

embankments on soft foundations. The optical setup and digital image processing used in this study is capable in evaluating the deformation patterns in the clay foundation beneath the embankment.

Geocell and wrap-around geosynthetic reinforcements installed at the base of the embankment are investigated. The provision of these reinforcements reduces horizontal displacements up to 50%. The increases in load capacities in terms of improvement ratio are 3 for geocell and 6.5 for wrap-around geosynthetic reinforcement. However, geocell reinforcement is more effective in minimizing differential settlements between the centerline and crest of the embankment.

The results of this study provide data for calibrating load-deformation numerical models that will be developed. These numerical models coupled with thermal numerical models will be used for further studies of the performance of various types of reinforced embankments on thawed peat land and degraded permafrost and for analysis of the field performance of reinforced embankments.

ACKNOWLEDGEMENTS

Funding of this research is provided by the University of Manitoba under the University Research Grant Program. Dr. Jinyuan Liu (Ryerson University) provided valuable guidance in setting up the tests. The authors are grateful to Mr. Kerry Lynch for his assistance in the test set up. The first author is grateful to the Ministry of Higher Education, Malaysia and Universiti Tun Hussein Onn Malaysia for funding his studies.

REFERENCES

Adam MT and Collin JG (1997) Large model spread footing load tests on geosynthetic reinforced soil foundations. Journal of Geotechnical and Geoenvironmental Engineering, January :66-72

Almeida MSS., Britto AM and Parry RHG (1986) Numerical modelling of a centrifuged embankment on soft clay. Canadian Geotechnical Journal, 23: 103-114.

Gill D and Lehane B (2001) An optical technique for investigating soil displacement patterns. Geoteh. Testing J., ASTM, 24(3): 324-329.

Gill D and Lehane B (2004) Displacement fields induced by penetrometers installation in an artificial soil. International Journal of Physical Modelling and Geotechnics, 1: 25-36.

Goodman, JW (1975). Statistical properties of laser speckle patterns. In: Laser Speckle and Related Phenomena, Dainty (ed.), Springer Verlag :9-75.

Indraratna B, Balasubramaniam AS, and Balachandran S (1992) Performance of test embankment constructed to failure on soft marine clay. Journal of Geotechnical Engineering, 118(1):12-32.

Iskander M, and Liu J (2010) Spatial deformation measurement using transparent soil. Geotechnical Testing Journal, 33 (4):1-8.

Iskander MG, Sadek S and Liu J (2002) Optical measurement of deformation using transparent silica gel to model sand. IPJMG- Intl. J. of Physical Modelling in Geotechnics, 4:13-26.

Krishnaswamy NR, Rajagopal K, Madhavi Latha G, (2000) Model studies on geocell supported embankments constructed over soft clay foundation. Geotech. Testing J., ASTM 23: 45–54.

Liu J (2003) Visualization of 3-D Deformation using Transparent Soil Models. PhD Dissertation, Polytechnic University, U.S.A.

Mannheimer RJ, and Oswald C (1993) Development of transparent porous media with permeabilities and porosities comparable to soils, aquifers, and petroleum reservoirs. Ground Water, 31(5):781–788.

McKelvey D (2002) The Performance of Vibro Stone Column Reinforced Foundations in Deep Soft Soil. PhD Thesis, Queen`s University at Belfast, Northern Ireland, U.K.

Mhaiskar SY and Mandal JN (1996) Investigations on soft clay subgrade strengthening using geocells. Construction and Building Material Journal, 10 (4):281-286.

Mohidin N, Alfaro MC and Masirin MIM (2010) Development of transparent clay for laboratory model tests. Proc. 63rd Canadian Geotechnical Conf. and the 6th Canadian Permafrost Conference (GEO2010 Calgary), Calgary.: 12-16.

Palmiera EM (2012). Embankments. Chapter 5, Handbook of Geosynthetic Engineering (Shukla, S.K.-Editor). ICE Publishing, London, 101-127.

Poungchompu P, Hayashi S, Suetsugu D, Du YJ and Alfaro MC (2010) Performance of raft and pile foundation on soft Ariake clay ground. Lowland Technology International 12(1): 41-46.

Sadek S, Iskander MG and Liu J (2003) Accuracy of digital image corelation for measuring deformation in transparent media. Journal of Computing in Civil Engineering, ACSE : 88-166

Sitharam TG, Sireesh S, and Dash SK (2005) Model studies of a circular footing supported on geocell-reinforced clay. Canadian Geotechnical Journal 42: 693-703.

Take WA, White DJ and Bolton MD (2003). Soil deformation measurement using particle image velocimetry (PIV) and photogrammetry. Geotechnique 53, (7) :619-631.

Wesseloo J, Visser AT, Rust E (2009). The stress – strain behavior of multiple geocell pack. Geotextile and Geomembranes 27: 31-38.